GIS and Lineament Analysis for Monitoring Geodynamic Activity in the Charvak Reservoir Region

Fazilova, D.,[1, 2, 3*] Magdiev, Kh.[1,4], and Rakhimberdieva, M.[5]
[1]Space Researches Laboratory, Ulugh Beg Astronomical Institute of Uzbekistan Academy of Sciences, Republic of Uzbekistan, E-mail: dil_faz@yahoo.com*
[2]Mine Surveying and Geodesy Department, Tashkent State Technical University Named after Islam Karimov, Republic of Uzbekistan
[3]Department of Natural Geography, National University of Uzbekistan Named after Mirzo Ulugbek, Republic of Uzbekistan
[4]Geoinformation System Management and Support Department, Cadaster Agency under Economy and Financial Ministry of Republic Uzbekistan, Republic of Uzbekistan, E-mail: hasan.magdiev@gmail.com
[5]Geodesy, Cartography and Cadaster Department, National University of Uzbekistan Named after Mirzo Ulugbek, Republic of Uzbekistan, E-mail: maftun.18.08@gmail.com
**Corresponding Author*

DOI: https://doi.org/10.52939/ijg.v21i7.4317

Abstract
This study introduces an innovative geospatial approach for monitoring seasonal geodynamic activity and seismic hazard in the Charvak Reservoir region of northeastern Uzbekistan an area characterized by inherited fault systems, frequent shallow earthquakes, and cyclic hydrological loading. Unlike previous studies that assess deformation using long-term seismicity or single-period imagery, this work integrates multi-temporal satellite remote sensing (Landsat-8), automated GIS-based lineament analysis, directional statistics, historical seismicity (1955–2024), and monthly water volume records. Lineament extraction was performed for three hydrological phases in 2024 March (low water), July (peak water), and September (drawdown) to capture the structural response to seasonal stress fluctuations. Results reveal a marked increase in lineament density during and after the peak water phase, particularly near active fault zones. Orientation patterns remained stable (NE–SW, E–W), aligning with regional tectonics, while density shifts indicated dynamic stress redistribution. Spatial overlay with seismic epicenters confirmed a strong correspondence between high-density lineament zones and localized deformation. Based on these multi-source indicators, five geodynamically active subzones were delineated, with the highest hazard concentration in the North Pskem and Kumbel-Kokand sectors. The key contribution of this study lies in applying a seasonal, lineament-based deformation monitoring framework previously untested in the Charvak region which enhances the understanding of reservoir-induced stress responses and provides a transferable model for georisk management in tectonically complex hydrosystems.

Keywords: Geodynamic activity, GIS analysis, Lineaments, Reservoir water level, Seismic zoning

1. Introduction

Reservoir-induced seismicity (RTS) illustrates how water level fluctuations can trigger fault reactivation and stress redistribution [1][2] and [3]. Significant RTS events include earthquakes at Xinfengjiang (1962, Mw 6.2), Kariba (1963, Mw 6.2), and Koyna (1967, Mw 6.3) [4][5] and [6]. Even moderate changes in reservoir levels have been linked to low-magnitude (Mw < 3) seismic activity [7]. Studies at Koyna [8] and the Three Gorges Reservoir [9] show that stress from water loading and fault geometry are key factors. These cases highlight the role of structural indicators in assessing geodynamic instability in reservoir-affected, tectonically active regions.

The Charvak Reservoir in Uzbekistan is a key water and energy resource and serves as a major tourist and recreational zone in the Tashkent region. Located at the confluence of the Chatkal, Pskem, and Koksu rivers, it lies within the tectonically active western Tian Shan. This region is characterized by high seismicity and complex fault systems, including the Pskem and Chatkal faults [10]. Recent studies have noted a rise in seismic activity and shoreline instability, potentially linked to water level fluctuations [11][12] and [13]. Geophysical and geodetic data suggest that reservoir-induced stress changes may influence local deformation and seismicity [14] and [15]. Landslides, such as the

Mingchukur event, have also become more frequent, associated with both hydrological and tectonic factors [16] and [17]. Given the reservoir's location in a tectonically active zone and its role as a densely visited recreational area, it is essential to assess geodynamic instability using advanced spatial analysis techniques.

One key indicator of geodynamic instability is the presence of lineaments linear geological features that reflect active faults, stress zones, and crustal deformations. Changes in lineament density and orientation over time are widely recognized as structural proxies for stress redistribution and crustal deformation. These indicators reflect surface responses to dynamic stress regimes, including both tectonic and hydrological loading [18][19] and [20]. For example, a recent study in the Charvak Reservoir region demonstrated that lineament density increases significantly during peak water storage phases, correlating with elevated pore pressure and possible fault reactivation [21]. Other research has shown that temporal variations in lineament orientation can act as seismic precursors, indicating early stages of stress accumulation before earthquake occurrence [22]. Furthermore, lineament analysis has proven effective for mapping evolving deformation fields in tectonically active terrains and identifying potential zones of instability [23] and [24]. Although this method does not quantify deformation rates directly unlike GNSS or InSAR it enables spatial localization of structurally sensitive zones and enhances early-warning capacity. In this study, seasonal variations in lineament patterns are used to evaluate surface responses to reservoir-induced stress fluctuations, offering a cost-effective approach to geodynamic monitoring in complex and hydrologically sensitive regions.

Despite growing attention to reservoir-triggered seismicity (RTS), there remains a significant research gap in understanding the seasonal geodynamic effects of water level fluctuations in tectonically complex regions. Most prior studies have focused either on long-term seismic trends or on individual high-magnitude events, often neglecting the subtler structural responses that occur over shorter hydrological cycles. The Charvak Reservoir area presents a particularly relevant case study due to its active fault systems, seasonal snowmelt-driven water input, and observed shoreline instability. This study addresses this gap by proposing an integrated geospatial framework that combines multi-temporal remote sensing, GIS-based lineament extraction, and historical seismicity records. The innovative contribution lies in the systematic mapping of lineament density and orientation at multiple seasonal stages, followed by quantitative spatial correlation with seismic epicenters and water volume records. This multi-layered approach, not previously applied to the Charvak region, offers new insight into how hydrological forcing interacts with active tectonic structures and provides a replicable methodology for geodynamic monitoring in reservoir-influenced settings. This study focuses on the year 2024, analyzing seasonal changes in lineament patterns and seismic activity around the Charvak Reservoir. The main tasks include: seismic zoning using an earthquake catalog; lineament mapping from Landsat 8 imagery; comparison of lineament patterns across different reservoir levels; and assessment of the relationship between active faults, water level fluctuations, and regional instability. The results will contribute to a better understanding of geodynamic processes in the area and support risk assessment related to structural changes.

2. Methodology

2.1 Study Area

The study area is located in the western Tian Shan, a seismically active region influenced by major fault systems such as the Pskem, Kumbel, Ugam, and Chatkal faults (Figure 1). Earthquake data from 1955 to 2024 were obtained from the Republican Center for Seismic Prognostic Monitoring (RCSPM) database [25]. Faults are taken from the database [26]. This tectonic environment, combined with hydrological fluctuations of the Charvak Reservoir, creates conditions favorable for induced seismicity and shoreline deformations Notably, calculated seismic intensity in some parts of the reservoir area has increased to IX on the MSK-64 scale, exceeding the baseline intensity of VIII [27]. The region is influenced not only by tectonic deformations but also by hydrological factors, including flash floods and mudflows [28].

Figure 2 illustrates the monthly variations in reservoir water volume during the period 2022–2024. A clear seasonal cycle is observed each year, with minimum volumes typically recorded between February and April (below 2,000 million m^3), followed by a sharp increase in late spring and early summer. Peak storage consistently occurs in July, exceeding 6,000 million m^3, and is followed by a gradual decline through autumn.

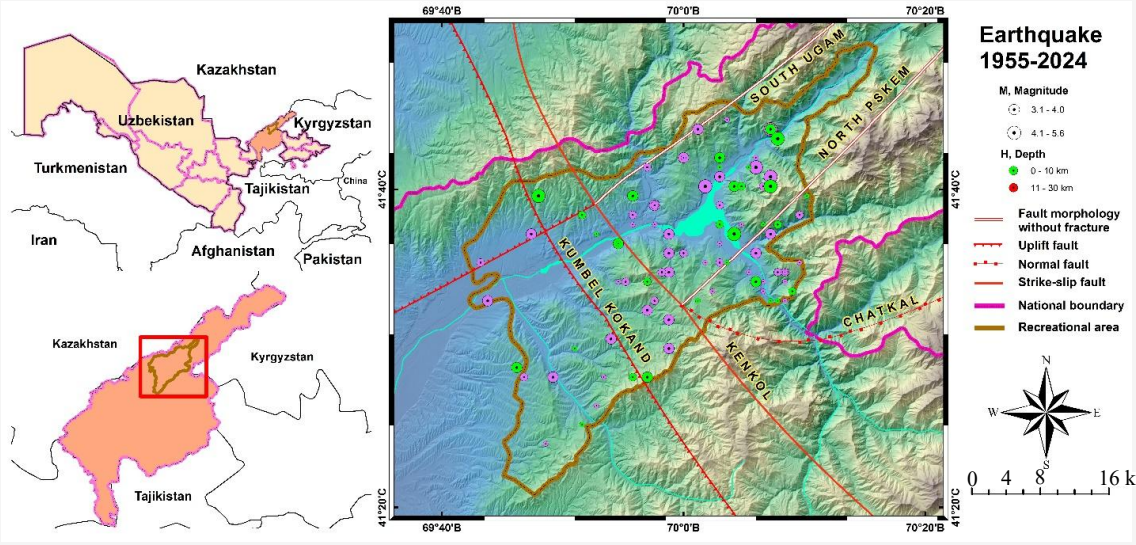

Figure 1: Charvak Reservoir region, Northeastern Uzbekistan

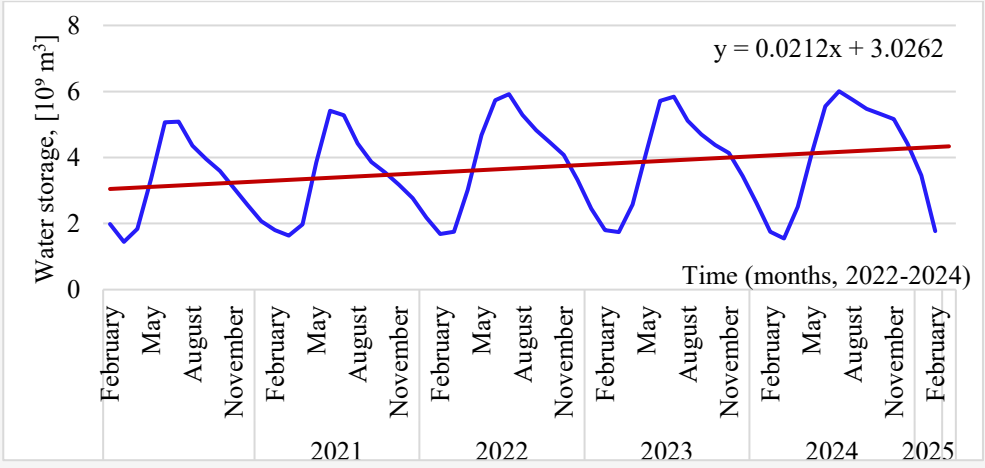

Figure 2: Monthly water storage [10^9 m³] in the Charvak Reservoir during 2022–2024. Data provided by the Dispatch Service of the Ministry of Water Resources of the Republic of Uzbekistan (internal archive, unpublished; personal communication, 2024)

In addition to these seasonal dynamics, the chart reveals a positive long-term trend in annual peak volumes, as indicated by the linear regression line. This suggests increasing hydrological loading over time, possibly due to climatic and operational factors. Based on this trend, the year 2024 was selected for detailed lineament analysis, as it exhibited the highest recorded maximum water volume and thus represents the period of strongest reservoir-induced stress conditions.

Seasonal fluctuations in reservoir water levels induce significant mechanical effects on adjacent crustal blocks. When water volume increases, the added hydrostatic load elevates vertical stress on reservoir margins and increases pore water pressure within faulted or fractured rock masses. According to poroelastic models [29] and [30], this reduces effective normal stress on fault planes and may promote slip or dilatation along pre-existing structural weaknesses. During the drawdown phase, stress unloading leads to relaxation and possible opening of shallow fractures due to elastic rebound. These cyclic loading and unloading effects are particularly pronounced in steep, fault-bounded zones near the reservoir shoreline and are known to influence both microseismic activity and the surface expression of deformation, such as increased lineament density and orientation shifts. The results observed in the Charvak region are consistent with such hydromechanical responses and reflect the interaction between seasonal hydrological forcing and active tectonic structures.

2.2 Seismic Risk Zoning Using Spline Interpolation in GIS

The use of Geographic Information Systems (GIS) provides significant value for geospatial modeling of seismic data due to the integration of spatial statistical analysis tools [31] and [32]. One of the effective interpolation methods for working with unevenly distributed point data is Spline interpolation. This mathematical approach makes it possible to create a continuous surface that reflects the spatial distribution of hazard by fitting a smooth curve that minimizes overall curvature. The biharmonic splines method belongs to the radial basis functions group and shares similarities with the thin plate spline approach. Spline interpolation is a mathematical technique that allows the creation of a continuous surface from a set of scattered points. This approach is useful when dealing with point data that is unevenly distributed across a study area and requires an estimate of the hazard distribution over the entire area. Spline interpolation is a mathematical technique that involves fitting a smooth curve to a set of data points by minimizing the overall curvature of the curve. For this purpose, we utilized the ArcGIS software tool. The algorithm used in the Spline tool applies Equation 1 to compute the interpolated surface function $S(x, y)$, which represents a smooth estimate of spatial variation based on known data points [33]:

$$S(x,y) = T(x,y) + \sum_{j=1}^{N} \lambda_j R(r_j)$$

Equation 1

Where:

j = 1,2...N,
N = number of points,
x,y = spatial coordinates,
λ_j = coefficients, obtained by solving a system of linear equations,
r_j = the distance from point (x,y) to point j,

Equation 2 defines the polynomial trend component of the spline function:

$$T(x, y) = a_1 + a_2x + a_3y$$

Equation 2

Where:

a_1, a_2, a_3 = coefficients, obtained by solving a system of linear equations.

Equation 3 represents the radial basis function $R(r_j)$, which depends on the distance r_j between the interpolation point and the known data point j:

$$R(r_j) = \frac{1}{2\pi}\left\{\frac{r_j^2}{4}\left[\ln\left(\frac{r_j}{2\pi}\right)+c-1\right]+\tau^2\left[K_0\left(\frac{r_j}{\tau}\right)+c+\ln\left(\frac{r_j}{2\pi}\right)\right]\right\}$$

Equation 3

Where:

τ^2 = a weight parameter equal to 0.1
K_0 = modified Bessel function
c = a constant equal to 0.577215.

The Spline interpolation method has been widely applied in studies related to seismic hazard mapping, as documented in [34][35][36] and [37]. The use of the complete time series of observations enables a more representative and reliable assessment of seismic risk. This approach helps identify persistent seismic hotspots, reveals long-term spatiotemporal patterns of seismic activity, and enhances the reliability of predictive models, particularly under conditions of sparse observation networks and a limited number of strong events in certain years. Since earthquakes with a magnitude below 2.0 are very weak, occur frequently on a daily basis, and are generally not felt by the population, only events with a magnitude greater than 3 were included in the analysis. Figure 3 presents the resulting seismic zoning maps based on the seismological data.

2.3 Satellite-Based Mapping of Lineament Structures

In this study, satellite imagery acquired by the Landsat 8 OLI & TIRS sensors from the United States Geological Survey (USGS) was used for the dates March 16, June 13, July 22, and September 24, 2024. The methodology for extracting lineament structures involved several sequential steps of multispectral data processing, starting with the preliminary correction of the Landsat 8 (L8) images. This stage plays a crucial role in digital image processing, as it reduces the impact of atmospheric distortions typical of optical remote sensing data [38]. Geometric correction of the source images was not required, as the USGS-provided data were already geometrically corrected and projected in UTM (WGS-1984, zone 42N). Therefore, the processing began with radiometric calibration followed by atmospheric correction, both performed in the ArcGIS 10.8 environment.

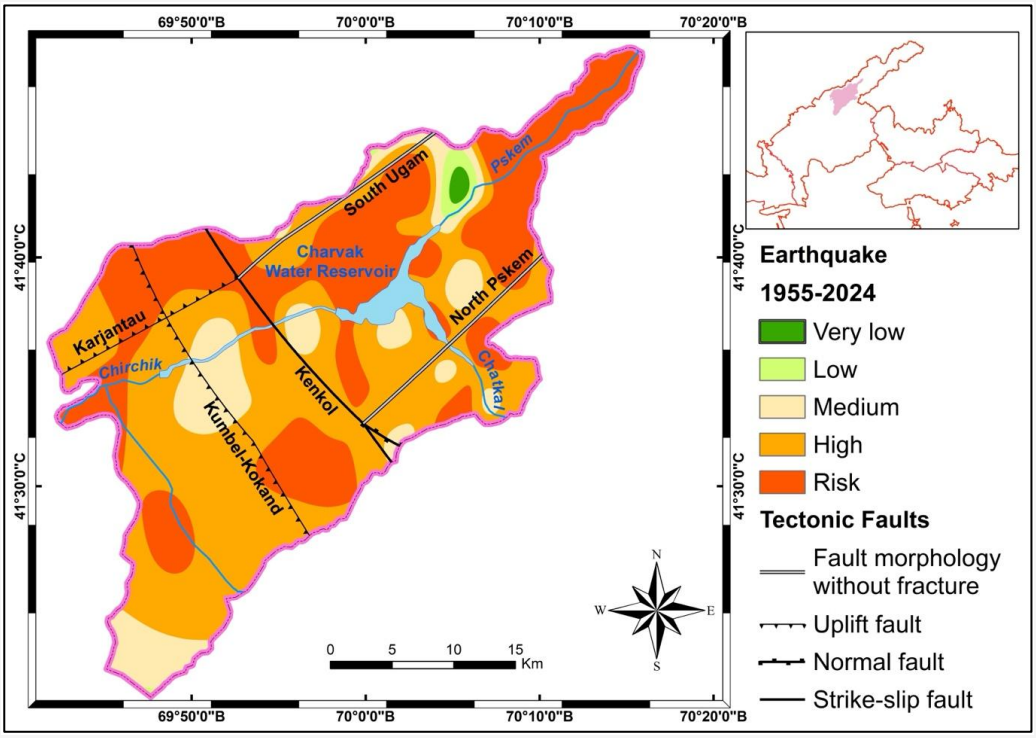

Figure 3: Seismic risk zoning of the Charvak tourist-recreational area based on earthquake data from 1955 to 2024

To enhance the accuracy of lineament extraction, it was necessary to determine the optimal combination of spectral bands. After a series of experiments with various image processing methods, classifications, and band combinations, it was found that the most prominent linear features were observed using the band ratio 6/2 (SWIR1/Blue). This choice is also supported by several other studies [39] and [40]. To improve spatial resolution and visual clarity, the SWIR1 and Blue bands (30 m resolution) were fused with the panchromatic band (15 m resolution) using the Pan-Sharpening tool in ArcGIS. This fusion method preserves the spectral characteristics of the original bands while enhancing spatial resolution to 15 m, significantly improving the clarity of geological structures [41].

Automatic extraction of lineament structures was performed using the PyLEFA software (v.0.61a) Lineament Extraction and Fracture Analysis [42]. The software's algorithm is based on mathematical morphology and factor analysis techniques [43], which facilitate the identification of linear features such as faults, boundaries, and folds. To increase edge detection accuracy, the Canny edge detection algorithm was applied with Gaussian noise filtering, reducing the impact of noise and enhancing boundary precision [44]. Subsequently, the Hough Transform was used to detect linear objects [45]. In PyLEFA, the user defines key Hough Transform parameters, including the minimum line length, permissible gap, coordinate discretization steps, and the number of detectable peaks (houghpeaks).

The lineament extraction process consists of the following stages: filtering to reduce noise and enhance contrast, application of the morphological gradient operator to refine object edges, skeletonization to define the central axis of linear features. The final stage included a geometric analysis of the lineaments (length, orientation, and shape), contextual evaluation based on neighboring pixels to verify detected features, and the creation of distribution density maps of lineament structures using ArcGIS 10.8.2. The use of GIS not only facilitated the visualization of seasonal lineament patterns but also enabled the spatial integration of multiple geodynamic indicators, including fault structures, seismicity, and reservoir dynamics. Lineament shapefiles generated in PyLEFA were imported into ArcGIS for density mapping and cross-layer analysis. Using GIS tools spline interpolation and zonal statistics on earthquake magnitude statistics, we extracted the output data as a raster and classified earthquake zones by risk level. Through spatial overlays and zonal statistics, we quantified the correspondence between lineament clusters and high seismic risk areas.

GIS tools also supported the classification of geodynamically distinct zones by aggregating information from different thematic layers such as epicenter distribution, fault proximity, and lineament density into a single spatial decision framework. This integrative capability of GIS proved essential for identifying structurally sensitive sectors and for developing region-specific hazard mitigation strategies.

3. Results and Discussion

Based on the earthquake catalog from 1955 to 2024 (Figure 1), seismic events in the Charvak tourist-recreational zone show a clear spatial correlation with major fault systems, including the Kumbel-Kokand, Chatkal, and Pskem faults. The map displays events with magnitudes ≥ 2.0, as these are considered most relevant from a hazard perspective. However, analysis of the complete catalog reveals a significant number of microseismic events with magnitudes below 2.0, indicating ongoing local activity along active faults. Depth distribution shows that most earthquakes occur in the upper crust (up to 15 km), while temporal analysis reveals an increase in recorded events in recent years. This underscores the need for continuous monitoring and integration of seismic and structural data within a GIS platform to support effective risk assessment.

The seismic zoning presented in Figure 3 is based on the analysis of the density and distribution of recorded earthquakes within the Charvak tourist-recreational area. As a result of spatial classification, zones of varying seismic risk levels were identified, ranging from very low to high. The highest risk areas are concentrated in the central part of the study region, particularly along the southern and southwestern shores of the reservoir, where a high concentration of epicenters and larger magnitude events have been recorded. These high-risk zones coincide with known active fault structures, confirming their geodynamic significance. Additionally, some of these zones overlap with areas of tourist and engineering infrastructure, highlighting the need for careful consideration in planning and site management. A comparison of the risk map with seasonal water level dynamics suggests that changes in hydrostatic pressure may intensify localized seismicity in the most affected areas. This underlines the importance of incorporating seismic risk assessments into spatial planning and risk management strategies, particularly in tourist-oriented regions.

Figure 4 presents seasonal lineament density maps (left) and corresponding rose diagrams of lineament orientation (right) for March, July, and September 2024. These data reveal spatiotemporal variations in structural lineaments within the Charvak tourist-recreational area, which may reflect seasonal changes in crustal stress influenced by reservoir water level fluctuations. In March, during the minimum water level phase (Figure 2), the highest lineament densities are concentrated in the southeastern part of the reservoir, particularly near the Kumbel and Kokand faults. This may indicate residual stress following the reduction in hydrostatic load. In July, at the peak water storage phase, zones of high lineament density expand northward and eastward, toward the Pskem region. This pattern suggests a structural response to increased hydrostatic pressure, potentially leading to fault reactivation or the development of secondary fractures. By September, during the drawdown phase, elevated lineament density persists in several key zones, indicating delayed or sustained stress responses. These observations may reflect the tectonic instability of localized crustal blocks even after the load begins to decrease.

Comparison with the seismic risk zoning map (Figure 3) reveals a notable spatial overlap between high lineament density zones and areas of elevated seismic hazard. This supports the interpretation that lineaments can serve as indicators of structurally sensitive and potentially active fault zones, especially under the influence of hydrological loading. The rose diagrams on the right side of Figure 4 illustrate the dominant orientation of lineaments for each season. Throughout the year, NE–SW and NW–SE directions prevail, aligning with the regional fault systems of the western Tian Shan. However, in July, a marked intensification of NE-trending lineaments is observed, likely associated with increased stress during maximum water levels. In September, the orientation remains consistent, indicating a structurally stable deformation regime with persistent tectonic activity.

To provide a more detailed characterization of the geodynamic setting of the study area, a conditional classification of zones was carried out based on a combination of indicators, including lineament density, seismic risk level, epicenter distribution, and structural features. As a result, five key geodynamic zones were identified, each differing in terms of activity level and potential hazard. Their main characteristics are summarized in Table 1. These findings highlight the relevance of integrating directional statistical methods with remote sensing and GIS tools to monitor structural dynamics in tectonically and hydrologically active areas. Such approaches contribute to better identification of geodynamicallly unstable zones and support spatial planning in regions with both geological and socio-economic significance.

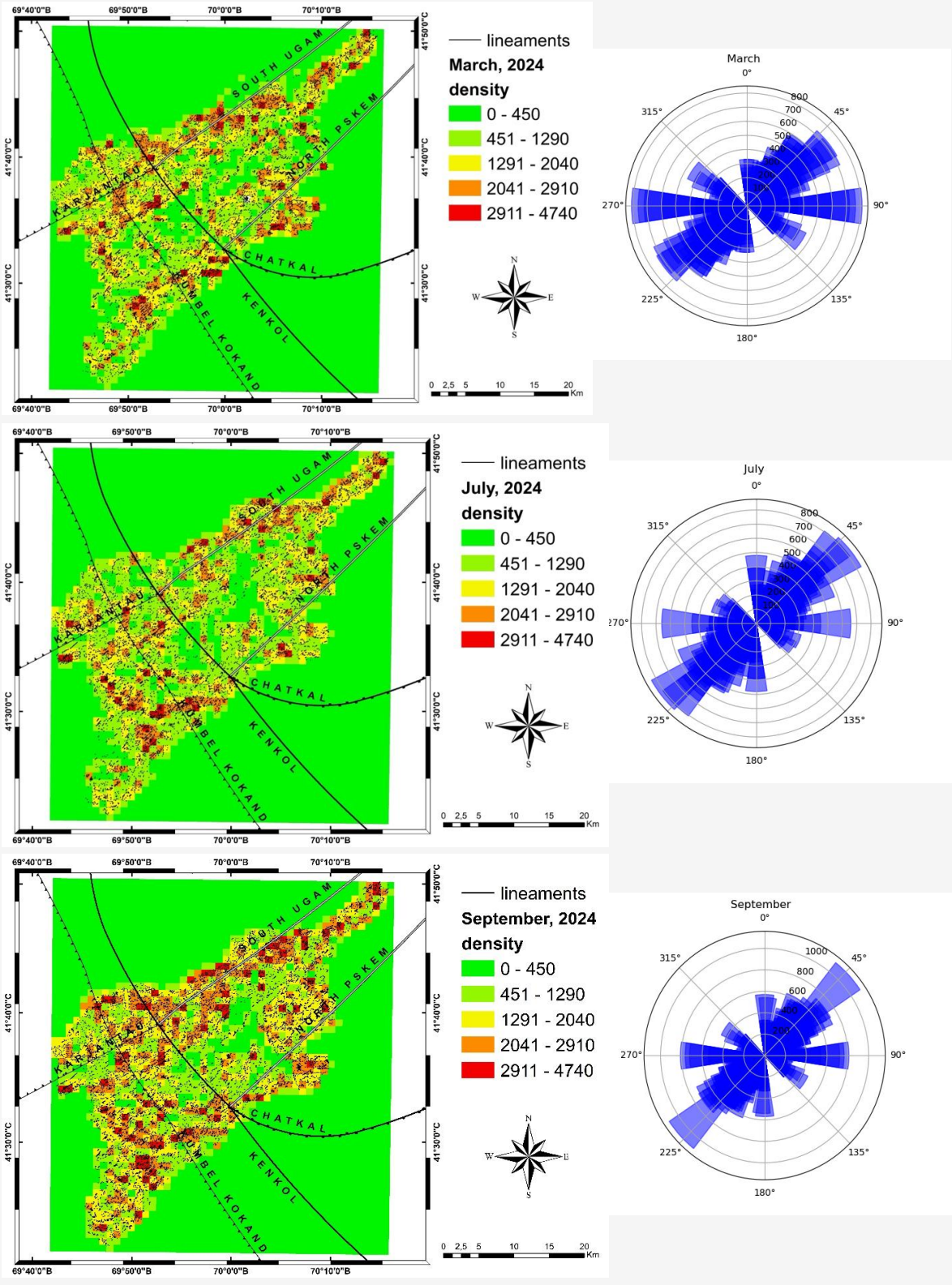

Figure 4: Spatiotemporal analysis of lineament density and orientation in the Charvak region during seasonal water level changes in 2024

Table 1: Geodynamic zones and their characteristics in the Charvak Reservoir

Zone	Location	Lineament Density	Seismic Risk Level	Dominant Faults	Observed Seismicity (Mw)	Notes
Southwest Shore	South and southwest of reservoir	High	High	Kumbel, Kokand	Up to 4.5	Overlap with infrastructure; active in all seasons
Northeast Sector	East and northeast of reservoir	Moderate–High	Moderate	Pskem	Mainly <3.5	Increased lineament density during peak water level (July)
Southeastern Area	Near Chatkal fault zone	High in spring	Moderate–High	Chatkal, Ugam	Up to 4.0	Stress response evident in March, suggesting residual deformation
Northwestern Periphery	Western slope of reservoir basin	Low–Moderate	Low	Secondary faults	<2.5	Relatively stable; minor seasonal structural variation
Central Basin Zone	Underwater central reservoir region	Moderate	Moderate–High	Assumed fault branches beneath the reservoir basin	Sparse data	Possible hidden structures; further study needed

4. Conclusion

This study demonstrates the value of integrating GIS-based lineament analysis, remote sensing, and seismic data to assess seasonal geodynamic activity and seismic hazard in the Charvak Reservoir region. By applying a multi-temporal framework based on Landsat-8 imagery, we identified spatial and directional variations in lineament systems that correspond with hydrological loading cycles. The highest lineament densities occurred during and after the peak water storage phase, suggesting that seasonal reservoir fluctuations contribute to surface stress redistribution and potential fault reactivation. Seismic risk zoning using historical earthquake data (1955–2024) delineated several high-hazard zones, notably in the southern and eastern sectors, which partially overlap with lineament clustering areas and contain critical infrastructure related to tourism and water resources. Directional statistical analysis confirmed persistent NE–SW and NW–SE trends aligned with regional tectonic structures, while seasonal variations in orientation reflect localized stress responses to changing hydrogeological conditions.

Based on structural, seismic, and hydrological indicators, five geodynamically distinct zones were classified, providing a foundation for spatially differentiated hazard assessment. The proposed methodology focusing on seasonal deformation proxies extracted from optical imagery offers a novel and cost-effective tool for tectonic risk monitoring in reservoir-influenced environments. It is particularly relevant for regions with limited access to continuous geodetic observations. The use of GIS-based analysis provides a powerful means to integrate diverse spatial datasets, visualize multi-temporal structural changes, and support evidence-based decision-making in hazard-prone areas. The findings support the integration of spatial analysis into early warning systems, infrastructure planning, and sustainable development strategies in the Charvak region and beyond. Future research should incorporate higher-resolution deformation monitoring (e.g., InSAR, continuous GNSS) to improve temporal sensitivity and deepen understanding of hydro-tectonic coupling in fault-prone hydrosystems.

Acknowledgements

This research was conducted as part of project No. AL-8624042530, supported by the Agency of Innovative Development under the Ministry of Higher Education, Science, and Innovation of the Republic of Uzbekistan. The authors also express their gratitude to the Dispatch Service of the Ministry of Water Resources of the Republic of Uzbekistan for providing valuable data on water volume variations in the Charvak Reservoir. Figures were prepared using the ArcGIS ver.10.8 graphic package. We also extend our gratitude to the reviewers for their constructive comments and valuable suggestions.

References

[1] Elliott, J. R., de Michele, M. and Gupta, H. K., (2020). Earth Observation for Crustal Tectonics and Earthquake Hazards. *Surveys in Geophysics*, Vol. 41, 1355–1389. https://doi.org/10.1007/s10712-020-09608-2.

[2] Gupta, H. K., (2022). Artificial Water Reservoir-Triggered Seismicity (RTS): Most Prominent Anthropogenic Seismicity. *Surveys in Geophysics*, Vol. 43(2), 619-659. https://doi.org/10.1007/s10712-021-09675-z.

[3] Büyükakpınar, P., Cesca, S., Hainzl, S., Jamalreyhani, M., Heimann, S. and Dahm, T., (2021). Reservoir-triggered Earthquakes Around the Atatürk Dam (Southeastern Turkey). *Frontiers in Earth Science*, Vol. 9. https://doi.org/10.3389/feart.2021.663385.

[4] Ge, S., Liu, M., Lu, N., Godt, J. W. and Luo, G., (2009). Did the Zipingpu Reservoir Trigger the 2008 Wenchuan Earthquake?. *Geophysical Research Letters*, Vol. 36. https://doi.org/10.1029/2009GL040349.

[5] Wilson, M. P., Foulger, G. R., Gluyas, J. G., Davies, R. J. and Julian, B. R., (2017). HiQuake: The Human-Induced Earthquake Database. *Seismological Research Letters*, Vol. 88, 1560–1565. https://doi.org/10.1785/0220170112.

[6] Gupta, H. K., (2002). A Review of Recent Studies of Triggered Earthquakes by Artificial Water Reservoirs with Special Emphasis on Earthquakes in Koyna, India. *Earth-Science Reviews*, Vol. 58, 279–310. https://doi.org/10.1016/S0012-8252(02)00063-6.

[7] Herath, P., Attanayake, J. and Gahalaut, K., (2022). A Reservoir Induced Earthquake Swarm in the Central Highlands of Sri Lanka. *Scientific Reports*, Vol. 12(1). https://doi.org/10.1038/s41598-022-22791-z.

[8] Gahalaut, K., Thai, A. T. and Rao, N. P., (2016). Rapid and Delayed Earthquake Triggering by the Song Tranh 2 Reservoir, Vietnam. *Bulletin of the Seismological Society of America*, Vol. 106(5), 2389–2394. https://doi.org/10.1785/0120160106,2-s2.0-84988970059.

[9] Jiayu, Z., Lili, Z., Yaowen, Z., Yunsheng, Y., Haoran, L., Yiming, D., Renlong, W. and Caixiong, H., (2022). Influence of the Three Gorges Reservoir Impoundment on Xiannvshan Fault Activity. *Geofluids*, Vol. 2023(1). https://doi.org/10.1155/2023/6611611.

[10] Plotnikova, L. M., Makhmudova, V. I. and Sigalova, O. B., (1992). Seismicity Associated with the Charvak Reservoir, Uzbekistan. *PAGEOPH*, Vol. 139, 607–608. https://doi.org/10.1007/BF00879953.

[11] Khamidov, L., Turapov, M., Mahkamov, S., Artikov, F. and Suyunov, S., (2021). Tracking the Local Seismicity Level in the Active Influence Zone of the Southern Uzbekistan Reservoirs. *Construction Mechanics, Hydraulics and Water Resources Engineering:* The International Scientific Conference, CONMECHYDRO- 2021, April 1-3, 2021, Tashkent, Uzbekistan. Vol. 264. https://doi.org/10.1051/e3sconf/202126402043.

[12] Umurzakov, R. A. and Muminov, M. Y., (2017). Studying of Kinematics and Elements of Tension of Blocks of the Massif According to Field Geological Observations. *World Journal of Mechanics*, Vol.7, 243-254. https://doi.org/10.4236/wjm.2017.79020.

[13] Fazilova, D. S. and Sichugova, L. V., (2021). *Deformation Analysis Based on GNSS Measurements in Tashkent Region*. *Supporting sustainable development by GIST:* The Annual International Scientific Conference on Geoinformatics, GI 2021, January 27-29, 2021, Tashkent, Uzbeksitan. Vol. 227. https://doi.org/10.1051/e3sconf/202122704002.

[14] Maksudov, S. K., Abdullabekov, K. N., Tuichiev, A. I. and Yusupov, V. R., (2021). Geomagnetic Field Variations Caused by the Processes Occurring at Different Depths in the Earth's Crust and Upper Mantle. *Izvestiya, Physics of the Solid Earth,* Vol. 57(3), 295-308. https://doi.org/10.1134/S1069351321020063.

[15] Khamidov, L., Artikov, F., Khamidov, K., Ganieva, B. and Anvarova, S., (2023). Seismicity Caused by Hydrological Regime of Large Reservoirs. *Construction Mechanics, Hydraulics and Water Resources Engineering:* The International Scientific Conference, CONMECHYDRO- 2022, August 23-24, 2022,

Tashkent, Uzbekistan. Vol. 365. https://doi.org/10.1051/e3sconf/202336503043.

[16] Juliev, M., Pulatov, A. and Hubl, J., (2017). Natural Hazards in Mountain Regions of Uzbekistan: A Review of Mass Movement Processes in Tashkent Province. *International Journal of Scientific & Engineering Research*, Vol. 8(2), 1102-1108.

[17] Kadirhodjaev, A., Kadavi, P. R., Lee, C. W. and Lee, S., (2018). Analysis of the Relationships between Topographic Factors and Landslide Occurrence and their Application to Landslide Susceptibility Mapping: a Case Study of Mingchukur, Uzbekistan. *Geosciences Journal*, Vol. 22(6), 1053–1067. https://doi.org/10.1007/s12303-018-0052-xS.

[18] Gabrielsen, R. H. and Olesen, O., (2024). The Concept of Lineaments in Geological Structural Analysis; Principles and Methods: A Review Based on Examples from Norway. *Geomatics*, Vol. 4(2), 189-212. https://doi.org/10.3390/geomatics4020011.

[19] Pavlin, G. B. and Langston, C. A., (1983). An Integrated Study of Reservoir-Induced Seismicity and Landsat Imagery at Lake Kariba, Africa. *Photogrammetric Engineering and Remote Sensing*, Vol. 49, 513-525.

[20] Chen, L. and Talwani, P., (2001). Mechanism of Initial Seismicity Following Impoundment of the Monticello Reservoir, South Carolina. *Bulletin of the Seismological Society of America*, Vol. 91(6), 1582-1594. https://doi.org/10.1785/0120000293.

[21] Sichugova, L. V. and Fazilova, D. S., (2020). Structural Interpretation of Lineaments Using Satellite Image Processing: A Case Study in the Vicinity of the Charvak Reservoir. *GI Support of Sustainable Development of Territories:* The International Conference InterCarto. InterGIS. September 24-29, 2020, Moscow, Russia. Vol. 26 (2), 436-442. https://doi.org/10.35595/2414-9179-2020-2-26-436-442.

[22] Sichugova, L. and Fazilova, D., (2021). The Lineaments as One of the Precursors of Earthquakes: A Case Study of Tashkent Geodynamical Polygon in Uzbekistan. *Geodesy and Geodynamics*, Vol. 12(6), 399-404. https://doi.org/10.1016/j.geog.2021.08.002.

[23] Nath, B., Singh, R. P., Gahalaut, V. K. and Singh, A. P., (2022). Dynamic Relationship Study between the Observed Seismicity and Spatiotemporal Pattern of Lineament Changes in Palghar, North Maharashtra (India). *Remote Sensing*, Vol. 14(1). https://doi.org/10.3390/rs14010135.

[24] Romero-Andrade, R., Trejo-Soto, M. E., Nayak, K., Hernández-Andrade, D., and Bojorquez-Pacheco, N., (2023). Lineament Analysis as a Seismic Precursor: The El Mayor Cucapah Earthquake of April 4, 2010 (MW7.2), Baja California, Mexico. *Geodesy and Geodynamics*, Vol. 14(2), 121–129. https://doi.org/10.1016/j.geog.2022.08.001.

[25] Earthquakes Database. *Republican Center for Seismic Forecasting Monitoring (RCSPM)*. [Online] Available: http://www.smrm.uz/?lang=ru. [Accessed: Jan. 7, 2025].

[26] Tsay, O., (2019). Electronic Map of Faults of the Middle, Southern Tien Shan and Adjacent Territories. *Fundamental Problems of Tectonics and Geodynamics:* LI Tectonic Meeting, 2019, Moscow, Russia: GEOS. Vol. 2, 382-386. [Online serial]. Available: http://www.ginras.ru/materials/files/MTS-2020-2%20.pdf. [Accessed: Feb. 2, 2025].

[27] Khusomiddinov, A., Yodgorov, S., Sadirov, F., Yadigarov, E., Aktamov, B. and Avazov, S., (2022). Estimation of the Seismic Intensity Increments in Tashkent Region. *Problems and Perspectives of Modern Science*: The 1st International Conference ICPPMS-2021, June 10-11, 2021, Tashkent, Uzbekistan. Vol. 2432(1). https://doi.org/10.1063/5.0089662.

[28] Aksenova L., Aitbaev D., Arifbaev A., Artikova F., Batalova I., Valieva V., Vakhidova G., Vidineeva E., Glazyrin G., Gorelkin N., Damladzhanov K., Dushdurova 3., Zhuraev B., Ivanov Yu., Kamaletdinova M., Kurbanov B., Kuchkarov Sh., Lesnik Yu., Li T., Mavlonov A., Magdiev Kh., Maksudov F., Mahamadaliev R., Mirzaliev T., Mode M., Nikiforova V., Nurbaev D., Popov V., Primov A., Rakhmatova N., Rakhmatov B., Rubinova F., Savello V., Saidova D., Saidova S., Semakova E., Sirlibaeva 3., Spektorman T., Sultanov A., Talipov H., Toychiev H., Tolkacheva G., Trofimov G., Turgunov H., Tursunov A., Umarov N., Umurzakov R., Frank L., Frolova N., Khikmatov F., Chub V., Egamberdiev A., Yunusov G., Yakubova N. (2008). Assessment of the Environment of Uzbekistan based on Environmental Indicators, 1st ed., Tashkent: GNPP Cartography. 57. [E-book]. Available: http://www.cawater-info.net/library/rus/uzbecoatlasru.pdf. [Accessed: Jan. 4, 2025].

[29] Biot, M. A., (1941). General Theory of Three-Dimensional Consolidation. *Journal Applied Physics*, Vol.12(2), 155–164. https://10.1063/1.1712886ff. ffhal-01368635.

[30] Do-Nascimento, A., Lunn, R. J. and Cowie, P., (2005). Numerical Modeling of Pore Pressure Diffusion in a Reservoir Induced Seismicity Site in Northeast Brazil. *Geophysical Journal International*, Vol.160(1), 249–262. http://doi.org/10.1111/j.1365-246X.2005.02473.x.

[31] Thammaboribal, P., Tripathi, N., and Lipiloet, S. (2024). Pre-Seismic Signature Detection using Diurnal GPS-TEC and Kriging Interpolation Maps (ASK-VTEC Technique): 11 May 2011, M9.0 Tohoku Earthquake Case Study. *International Journal of Geoinformatics*, Vol. 20(11), 148–161. https://doi.org/10.52939/ijg.v20i11.3715.

[32] Ramli, M. and Alias, N., (2024). Multidimensional Vulnerability Mapping Using GIS and Catastrophe Theory. *International Journal of Geoinformatics*, Vol. 20(8), 1–16. https://doi.org/10.52939/ijg.v20i8.3443.

[33] An Overview of the Interpolation Toolset. *ArcGIS Pro Geoprocessing Tool Reference*. [Online]. Available: https://pro.arcgis.com/ru/pro-app/3.0/tool-reference/spatial-analyst/how-spline-works.html. [Accessed: Jan. 4, 2025].

[34] Hervás, D., Carracedo, P. and Franco, G., (2025). Spatial Interpolation Model with Covariates Using Thin Plate Splines. *Decision Sciences: Second Decision Science Alliance International Summer Conference, Part I, DSA ISC 2024, Valencia, Spain, June 6–7, 2024*. 268 – 275. https://doi.org/10.1007/978-3-031-78238-1_25.

[35] Alavi, S. H., Bahrami, A., Mashayekhi, M. and Zolfaghari, M., (2024). Optimizing Interpolation Methods and Point Distances for Accurate Earthquake Hazard Mapping. *Buildings*, Vol. 14(6). https://doi.org/10.3390/buildings14061823.

[36] Hamdy, O., Gaber, H., Abdalzaher, M. S. and Elhadidy, M., (2022). Identifying Exposure of Urban Area to Certain Seismic Hazard Using Machine Learning and GIS: A Case Study of Greater Cairo. *Sustainability*, Vol. 14(17). https://doi.org/10.3390/su141710722.

[37] Fazilova, D., Makhmudov, M. and Magdiev, K., (2023). Analysis of Crustal Movements in the Angren-Almalyk Mining Industrial Area Using GNSS Data. *International Journal of Geoinformatics*, Vol. 19(11), 12–19. https://doi.org/10.52939/ijg.v19i11.2915.

[38] Tempfli, K., Kerle, N., Huurneman, G. C. and Janssen, L. L., (2009). *Principles of Remote Sensing*, 4th ed., The International Institute for Geo-Information Science and Earth Observation, (ITC), Enschede, The Netherlands.

[39] Mwaniki, M. W., Moeller, M. S. and Schellmann, G., (2015). A Comparison of Landsat 8(OLI) and Landsat 7 (ETM+) in Mapping Geology and Visualizing Lineaments: A Case Study of Central Region Kenya. *International Archives of the Photogrammetry, Remote Sensing and Spatial Information Sciences*, XL-7/W3, 897-903. https://doi.org/10.5194/isprsarchives-XL-7-W3-897-2015.

[40] Redouane, M., Mhamdi, H., Haissen, F., Raji, M. and Sadki, O., (2022). Lineaments Extraction and Analysis Using Landsat 8 (OLI/TIRS) in the Northeast of Morocco. *Open Journal of Geology*, Vol. 12, 333-357. https://doi.org/10.4236/ojg.2022.125018.

[41] Zhang, Y., (2002) A New Automatic Approach for Effectively Fusing Landsat 7 as Well as IKONOS Images: *Proceedings of the IEEE International Geoscience and Remote Sensing Symposium*, IGARSS'02, Toronto, ON, Canada, June 24–28, 2002.

[42] Shevyrev, S. and Carranza, E. J. M., (2020). Modelling of Geodynamic Regimes of Precious Metal-bearing Porphyry Deposits: Lazurnoe Deposit (Sikhote–Alin Belt, Far East) Case Study. *Geological Journal*, Vol. 55 (12), 8309-8328. https://doi.org/10.1002/gj.3935.

[43] Shevyrev, S. and Boriskina, N., (2025). Analysis of Structural Position of Carlin-Type Gold Deposits with Lineament Analysis of Remote Sensing Data Using pyLEFA Software. *Minerals*, Vol. 15(3). https://doi.org/10.3390/min15030219.

[44] Canny, J., (1989). A Computational Approach to Edge Detection. *IEEE Transactions on Pattern Analysis and Machine Intelligence*, Vol. PAMI-8(6), 679-698. https://doi.org/10.1109/TPAMI.1986.4767851.

[45] Duda, R. O. and Hart, P. E., (1972). Use of the Hough Transformation to Detect Lines and Curves in Pictures. *Communications of the ACM*, Vol.15, 11–15. https://doi.org/10.1145/361237.361242.